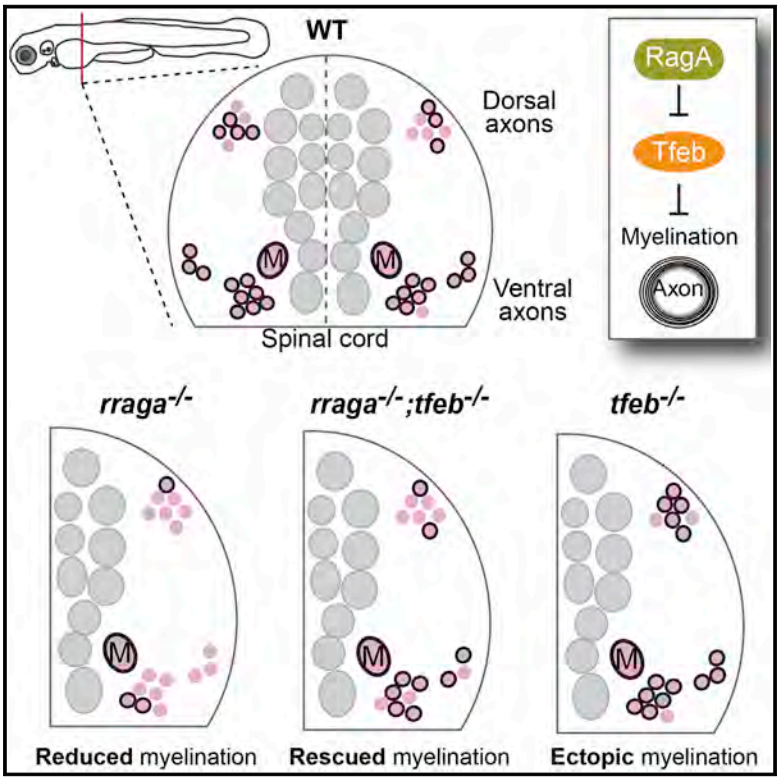
Article

Developmental Cell

The Lysosomal Transcription Factor TFEB Represses Myelination Downstream of the Rag-Ragulator Complex

Graphical Abstract



Highlights

- RagA is required autonomously in oligodendrocytes for CNS myelination in zebrafish
- Inactivation of Tfeb rescues the myelin defect in RagA mutants
- Tfeb mutants exhibit ectopic myelination, showing that Tfeb represses myelination
- During remyelination in mammals, TFEB localizes to the cytoplasm, where it is inactive

Authors

Ana M. Meireles, Kimberle Shen, Lida Zoupi, Harini Iyer, Ellen L. Bouchard, Anna Williams, William S. Talbot

Correspondence

william.talbot@stanford.edu

In Brief

Using genetic approaches in zebrafish, Meireles and Shen et al. show that the lysosomal regulators RagA and Tfeb have opposing roles to regulate myelin formation. Tfeb represses myelination, and RagA represses Tfeb. In RagA mutants, Tfeb is hyperactive, and myelin is nearly eliminated.

Meireles et al., 2018, Developmental Cell *47*, 319–330
November 5, 2018 © 2018 Elsevier Inc.
https://doi.org/10.1016/j.devcel.2018.10.003

CellPress

Developmental Cell
Article

The Lysosomal Transcription Factor TFEB Represses Myelination Downstream of the Rag-Ragulator Complex

Ana M. Meireles,[1,3] Kimberle Shen,[1,3,4] Lida Zoupi,[2] Harini Iyer,[1] Ellen L. Bouchard,[1] Anna Williams,[2] and William S. Talbot[1,5,*]

[1]Department of Developmental Biology, Stanford University School of Medicine, Stanford, CA 94305, USA
[2]University of Edinburgh/MS Society Centre for MS Research, MRC Centre for Regenerative Medicine, University of Edinburgh, Edinburgh Bioquarter, 5 Little France Drive, Edinburgh EH16 4UU, UK
[3]These authors contributed equally
[4]Present address: Genentech, Inc., 1 DNA Way, South San Francisco, CA 94080, USA
[5]Lead Contact
*Correspondence: william.talbot@stanford.edu
https://doi.org/10.1016/j.devcel.2018.10.003

SUMMARY

Myelin allows for fast and efficient axonal conduction, but much remains to be determined about the mechanisms that regulate myelin formation. To investigate the genetic basis of myelination, we carried out a genetic screen using zebrafish. Here, we show that the lysosomal G protein RagA is essential for CNS myelination. In *rraga*$^{-/-}$ mutant oligodendrocytes, target genes of the lysosomal transcription factor Tfeb are upregulated, consistent with previous evidence that RagA represses Tfeb activity. Loss of Tfeb function is sufficient to restore myelination in RagA mutants, indicating that hyperactive Tfeb represses myelination. Conversely, *tfeb*$^{-/-}$ single mutants exhibit ectopic myelin, further indicating that Tfeb represses myelination during development. In a mouse model of de- and remyelination, TFEB expression is increased in oligodendrocytes, but the protein is localized to the cytoplasm, and hence inactive, especially during remyelination. These results define essential regulators of myelination and may advance approaches to therapeutic remyelination.

INTRODUCTION

Myelin, the membranous sheath that insulates axons in vertebrates, is essential for both rapid conduction of action potentials and for metabolic and trophic support of axons (Fünfschilling et al., 2012; Sherman and Brophy, 2005; Simons and Nave, 2015). Oligodendrocytes mature from oligodendrocyte precursor cells (OPCs), some of which differentiate during development, while others persist into adulthood (Emery, 2010). Adult OPCs can differentiate into myelinating oligodendrocytes to form new myelin in the adult brain, which occurs in response to motor learning in the healthy brain and also in diseases such as multiple sclerosis (MS) (Almeida and Lyons, 2017; Bengtsson et al., 2005; McKenzie et al., 2014; Münzel and Williams, 2013). MS results from inflammatory disruption of myelin in the central nervous system (CNS). Demyelination and irreversible axon loss in MS lead to impaired vision, loss of coordination, muscle weakness, fatigue, and cognitive impairment (Browne et al., 2014; Dutta and Trapp, 2011; Franklin and Ffrench-Constant, 2008; Münzel and Williams, 2013). Despite the importance of myelination in the healthy and diseased CNS, the molecular mechanisms that control oligodendrocyte development are only partly understood.

Lysosomes, long recognized as degradative organelles in the cell, are emerging as important signaling hubs that integrate nutrient availability with specialized cellular functions (Appelqvist et al., 2013; Ferguson, 2015; Saftig and Haas, 2016; Settembre and Ballabio, 2014; Settembre et al., 2013). Biochemical studies have defined the roles of several essential lysosomal proteins in the context of nutrient sensing and regulation of metabolic pathways (Efeyan et al., 2015). For example, in the presence of amino acids, guanosine triphosphate (GTP)-bound heterodimeric Rag-GTPases (RagA or B bound to Rag C or D) recruit mTORC1 to the lysosomal membrane, where it is then activated to induce protein synthesis and cell growth (Kim et al., 2008; Sancak et al., 2008; Shaw, 2008). This process requires the guanine nucleotide exchange factor (GEF) activity of the Ragulator complex, encoded by the *lamtor* genes (Bar-Peled et al., 2012; Sancak et al., 2010). Additionally, RagA regulates the activity of transcription factor EB (TFEB), which controls lysosomal biogenesis and autophagy (Sardiello, 2016; Sardiello et al., 2009; Settembre et al., 2011). When nutrients are available and lysosomal activity is sufficient, RagA recruits TFEB to the lysosome, where it is phosphorylated and inactivated. When the cell is starved or when lysosomal activity is disrupted or insufficient, TFEB is dephosphorylated, allowing it to enter the nucleus and activate target genes that control lysosome biogenesis, autophagy, and lipid catabolism (Martina and Puertollano, 2013; Napolitano and Ballabio, 2016). In addition to controlling lysosomal activity in phagocytic cells (Shen et al., 2016), RagA and RagB also function in cardiomyocytes, underscoring the important roles of the lysosomes in diverse cell types (Kim et al., 2014). Moreover,

TFEB activation promotes clearing of intracellular debris in laboratory models of neurodegenerative diseases such as Huntington's disease (Appelqvist et al., 2013; Martini-Stoica et al., 2016; Williams et al., 2008), but the roles of RagA and TFEB in other aspects of CNS development and disease remain unexplored.

Starting with a forward genetic screen in zebrafish, we define essential functions for several key lysosomal signaling molecules in myelination. We show that mutations in *rraga* or the Ragulator component *lamtor4* result in reduced CNS myelination. We find that Tfeb target genes are significantly upregulated in myelinating glia of *rraga*$^{-/-}$ mutants. Consistent with the hypothesis that increased Tfeb activity blocks myelination in *rraga*$^{-/-}$ mutants, elimination of *tfeb* activity rescues myelination in *rraga*$^{-/-}$ mutants. Additionally, in *tfeb*$^{-/-}$ mutants, we observe ectopic myelination in the dorsal spinal cord and ectopic expression of myelin basic protein (MBP) in the hindbrain. Moreover, transient overexpression of a nonphosphorylatable Tfeb construct represses *mbp* mRNA expression, further demonstrating that *tfeb* represses myelination in the developing CNS. We also explored the possibility that TFEB may be regulated during remyelination after injury. We find that localization of TFEB to the cytoplasm of oligodendrocytes (where it is inactive as a transcription factor) increases during remyelination in a mouse model of focal demyelination. Together, our results reveal essential roles for RagA and TFEB in regulating myelination and suggest that manipulation of TFEB or its downstream effectors may represent a new avenue for improving therapeutic remyelination in MS.

RESULTS

The Rag-Ragulator Complex Is Essential for CNS Myelination

In a forward genetic screen using zebrafish, we identified *rraga* and *lamtor4*, which encode RagA and the Ragulator component Lamtor4, respectively, as genes essential for microglia development (Shen et al., 2016). To examine myelination in zebrafish carrying mutations in these genes, we analyzed the expression of the myelin markers *myelin basic protein* (*mbp*) and *proteolipid protein* (*plp1b*) by in situ hybridization (ISH). Homozygous *rraga*$^{-/-}$ mutants exhibited reduced *mbp* mRNA expression in the CNS (Figure 1A, white arrows), whereas *mbp* expression in the peripheral nervous system (PNS) was normal (Figure 1A, black arrows). Similarly, expression of *plp1b* mRNA was reduced in *rraga*$^{-/-}$ homozygous mutants (Figure 1B). As described previously (Shen et al., 2016), *lamtor4*$^{-/-}$ homozygous mutants and rraga$^{-/-}$ mutants have very similar phenotypes (Figure S1).

Previous biochemical studies have provided evidence that the Rag-Ragulator complex recruits mTORC1 to lysosomes, where it is activated in response to amino acids (Napolitano and Ballabio, 2016; Sancak et al., 2010). To determine if reduced mTORC1 activity might cause the reduction of myelin in *rraga*$^{-/-}$ mutants, we compared the phenotypes of *rraga*$^{-/-}$ and *mtor*$^{-/-}$ mutants using the previously identified *mtor*^{xu015} insertional allele (Ding et al., 2011). This analysis revealed important differences in the *rraga*$^{-/-}$ and *mtor*$^{-/-}$ mutant phenotypes. *mtor*$^{-/-}$ mutants exhibited a slight delay in overall development and partial reduction in *mbp* expression both in the CNS and PNS (Figure 1C), whereas *rraga*$^{-/-}$ mutants exhibited a strong, CNS-specific reduction of *mbp* expression (Figure 1A). In addition, treatment of wild-type zebrafish with Torin1, a potent and specific inhibitor of mTOR signaling (Thoreen et al., 2012), led to an overall developmental delay and slight reduction of *mbp* expression in both CNS and PNS, similar to *mtor*$^{-/-}$ mutants (Figure S2). Collectively, these experiments show that *mtor*$^{-/-}$ mutants express nearly normal levels of *mbp* in the CNS, in contrast to the strong and specific reduction of *mbp* in the CNS that is evident in *rraga*$^{-/-}$ mutants. These phenotypic studies indicate that the Rag-Ragulator complex has a role in oligodendrocyte myelination that is independent of mTOR.

RagA Acts Autonomously in Oligodendrocytes

To determine the cellular basis of RagA function in CNS myelination, we transiently expressed full-length wild-type *rraga* mRNA in *rraga*$^{-/-}$ mutants under the control of different cell type-specific regulatory sequences. Expression of *mbp* was rescued in *rraga*$^{-/-}$ mutants when the wild-type *rraga* gene was expressed in oligodendrocytes (*claudink* promoter) but not when expressed in neurons or microglia (*huc* or *mpeg* promoter, respectively) (Figures 1D and 1E). Previous transcriptomic studies in mammals show that *Rraga* expression increases in myelinating oligodendrocytes, consistent with its cell autonomous function in myelination (Marques et al., 2016). Combined with our previous analysis of microglia (Shen et al., 2016), these results indicate that RagA has independent and cell autonomous functions in oligodendrocytes and microglia.

Myelin Is Reduced, but Oligodendrocytes Are Present in *rraga*$^{-/-}$ Mutants

To determine if myelin ultrastructure is disrupted in *rraga*$^{-/-}$ mutants, we performed transmission electron microscopy on transverse sections of the ventral spinal cord in wild-type and *rraga*$^{-/-}$ mutant zebrafish. At 5 days post fertilization (dpf), wild-type siblings had approximately 4-fold more myelinated axons than *rraga*$^{-/-}$ mutants (Figure 2A). At 9 dpf, the number of myelinated axons increased in wild-type siblings, whereas no additional myelinated axons were detected in *rraga*$^{-/-}$ mutants (Figure 2B). *rraga*$^{-/-}$ mutants and their wild-type siblings had similar numbers of myelinated axons in the posterior lateral line nerve, which is a component of the PNS (Figure 2C). This ultrastructural analysis of *rraga*$^{-/-}$ mutants confirms that RagA is essential for myelination in the developing CNS, but not the PNS.

To determine if CNS myelin is reduced because *rraga*$^{-/-}$ mutants have fewer oligodendrocytes than wild-type, we examined the expression of *olig2*. Expression of *olig2* mRNA, which marks motor neurons and cells of the oligodendrocyte lineage (Ravanelli and Appel, 2015; Zhou and Anderson, 2002), was normal in *rraga*$^{-/-}$ mutants at 3 dpf, as detected by ISH (Figure S3A). Similarly, analysis of the transgenic reporter *Tg(olig2:GFP)* (Shin et al., 2003) at 4 dpf showed that the number and distribution of *olig2*-GFP-expressing cells were comparable between *rraga*$^{-/-}$ mutants and their wild-type siblings (Figure 2D).

To examine later stages of oligodendrocyte development, we used the transgenic reporter line *Tg*(*claudink:EGFP*), which expresses GFP in mature oligodendrocytes and Schwann cells (myelinating glia of the PNS) (Münzel et al., 2012). The *claudink:EGFP* reporter is expressed in the CNS of *rraga*$^{-/-}$ mutants, but at lower levels than in wild-type siblings (Figures 2E and

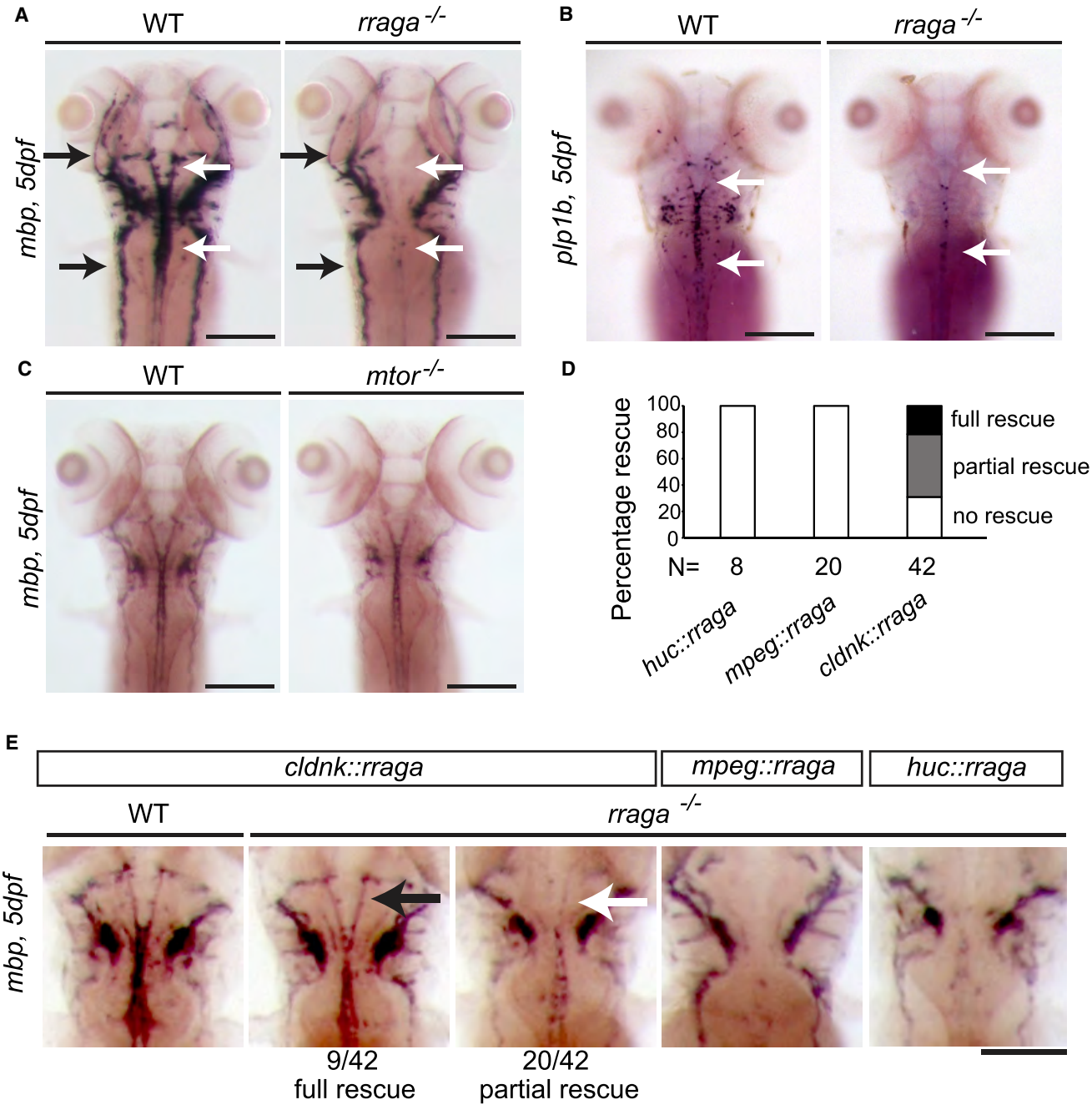


Figure 1. *rraga* Is Essential for CNS Myelination and Acts Autonomously in Oligodendrocytes

(A–E) Analysis of *mbp* or *plp1b* mRNA expression at 5 dpf by whole mount in situ hybridization.

(A) Compared to their wild-type siblings, *rraga*$^{-/-}$ mutants show reduced *mbp* expression in the CNS (white arrows), whereas *mbp* expression in the PNS is normal (black arrows).

(B) Expression of *plp1b* is also reduced in *rraga*$^{-/-}$ mutants. See also Figure S1.

(C) *mtor*$^{-/-}$ mutants are developmentally delayed and have a small reduction in *mbp* mRNA expression levels in the CNS and PNS. See also Figure S2.

(D) Quantification of rescue of *mbp* expression in *rraga*$^{-/-}$mutants following expression of wild-type *rraga* under the control of the *claudink, mpeg* (expressed in macrophages), or *huc* promoter (expressed in neurons).

(E) Whole mount in situ hybridization analysis of *mbp* mRNA expression in 5-dpf *rraga*$^{-/-}$ mutants following expression of wild-type *rraga* under the control of different tissue-specific promoters. *mbp* mRNA expression is partially or fully rescued only when wild-type *rraga* is expressed in oligodendrocytes (*claudink* promoter).

All panels show dorsal views, with anterior to the top. Genotypes of all animals shown were determined by PCR after imaging. Scale bar, 50 μm.

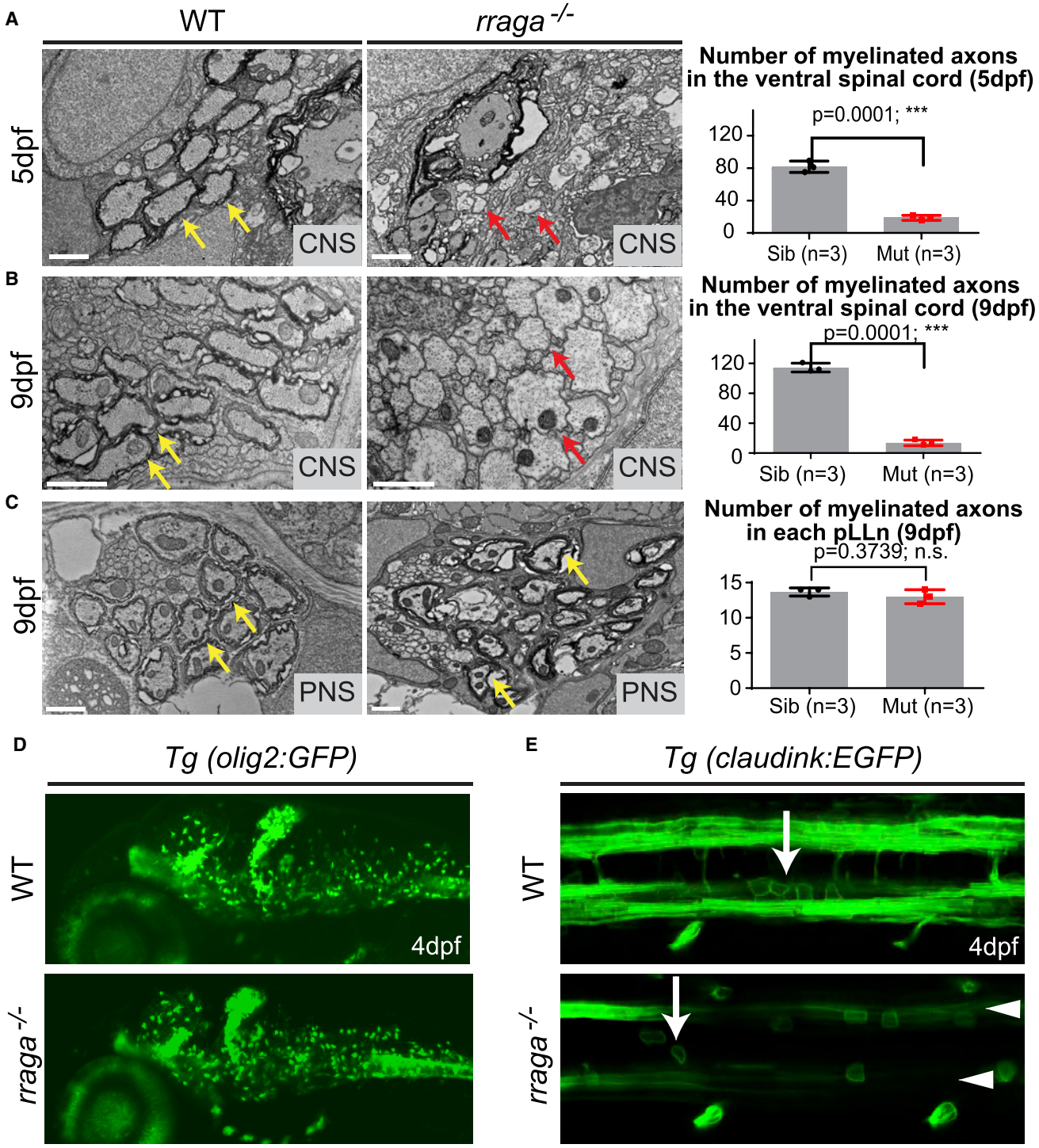


Figure 2. CNS Myelination Is Severely Reduced in *rraga*$^{-/-}$ Mutants although Oligodendrocytes Are Present

(A and B) TEM images of transverse sections of the ventral spinal cord (CNS) at 5 dpf (A) and 9 dpf (B) show fewer myelinated axons in *rraga*$^{-/-}$ mutants (middle panel) compared to wild-type siblings (left panel). Quantification of the number of myelinated axons in the ventral spinal cord at 5 dpf and 9 dpf is shown on the right; bar graph depicts average values and standard error; individual measurements are also shown.

(C) TEM images of transverse sections of the posterior lateral line nerve (pLLn) at 9 dpf show normal myelination in *rraga*$^{-/-}$ mutants (middle panel) compared to the wild-type sibling (left panel). Quantification of the number of myelinated axons in the pLLn at 9 dpf is shown on the right; bar graph depicts average values and standard error; individual measurements are also shown. In A–C, red arrows indicate unmyelinated axons, and yellow arrows indicate myelinated axons. 3 wild-type and 3 *rraga*$^{-/-}$ mutants were analyzed. Scale bar, 1 μm. (***p < 0.001; Student's t test, two-tailed).

(legend continued on next page)

S3B). In agreement with the *olig2* marker analysis, oligodendrocyte cell bodies are visible in both *rraga*$^{-/-}$ mutants and their wild-type siblings (arrows), but in *rraga*$^{-/-}$ mutants, the myelinating processes that normally extend along the axonal tracts are severely reduced (Figure 2E, arrowheads). These studies indicate that cells of the oligodendrocyte lineage are present in *rraga*$^{-/-}$ mutants and that the onset of myelination is disrupted.

Transcriptomic Analysis Reveals Upregulation of Lysosomal Genes and Tfeb Targets in Myelinating Glia of *rraga*$^{-/-}$ Mutants

To investigate the pathways that are disrupted in myelinating glia of *rraga*$^{-/-}$ mutants, we conducted RNA sequencing of FACS-sorted *Tg*(*claudink:GFP*)-expressing cells from wild-type and *rraga*$^{-/-}$ mutant larvae at 5 dpf. *claudink* is expressed in oligodendrocytes and Schwann cells (Münzel et al., 2012), but because myelin appears to be normal in the PNS of *rraga*$^{-/-}$ mutants (Figures 1A and 2E), differences detected in *Tg*(*claudink:GFP*)-expressing cells are likely to reflect changes in the oligodendrocyte transcriptome. Comparison of wild-type and *rraga*$^{-/-}$ mutant samples revealed 343 genes significantly upregulated in *Tg*(*claudink:GFP*)-expressing cells of *rraga*$^{-/-}$ mutants (>2.5× ; $p < 0.01$) and 298 significantly downregulated genes (<2.5×; $p < 0.01$) (Figure 3A; Tables S1, S2, and S3). Consistent with the reduction of myelination in the CNS of *rraga*$^{-/-}$ mutants, expression of myelin genes including *plp1b* and *myelin protein zero (mpz)* was significantly reduced (Figure 3A). Also consistent with our observation that PNS myelin is normal in *rraga*$^{-/-}$ mutants, the key regulators of Schwann cell myelination *egr2b* and *pou3f1* are expressed at similar levels in wild-type and *rraga*$^{-/-}$ mutants.

Functional annotation with PANTHER (Mi et al., 2013, 2017) revealed that genes associated with lysosomal activities were significantly enriched within the upregulated genes in *rraga*$^{-/-}$ mutant myelinating glia (Gene Ontology [GO] term: cellular component; Table S1). TFEB directly activates the expression of more than 400 genes involved in lysosomal biogenesis, autophagy, mitophagy, lipid catabolism, and lysosomal biogenesis (Medina et al., 2011; Napolitano and Ballabio, 2016; Nezich et al., 2015; Palmieri et al., 2011; Settembre et al., 2011). We compared our lists of genes differentially expressed in myelinating glia of *rraga*$^{-/-}$ mutants (upregulated and downregulated) to a previously compiled list of TFEB target genes (Palmieri et al., 2011). 17 previously defined TFEB target genes were upregulated in myelinating glia of *rraga*$^{-/-}$ mutants, including *ctsa*, *ctsba*, *atp6ap1b*, *agtrap*, *hexb*, *and sqstm1* (Figure 3A and Table S3). Similar analysis identified 4 TFEB target genes in the downregulated dataset, namely *hoxc13a*, *prkag2b*, *naglu*, and *comtd* (Figure 3A and Table S3).

Confirming and extending our analysis of TFEB target gene expression in myelinating glia, we performed quantitative RT-PCR on total RNA from wild-type and *rraga*$^{-/-}$ mutants. Our analysis of 21 well-established TFEB target genes (Palmieri et al., 2011) confirmed that *ctsba*, *ctsa*, *and sqstm1* are significantly upregulated in *rraga*$^{-/-}$ mutants and identified 9 more TFEB target genes upregulated in whole-animal RNA samples, including *gla*, *hexa*, *lamp1a*, *psap*, *clcn7*, *gba*, and *neu* (Figure S4A). Taken together, these experiments provide evidence that TFEB target genes are upregulated in oligodendrocytes of *rraga*$^{-/-}$ mutants, consistent with previous reports demonstrating that RagA represses TFEB in other cell types (Martina and Puertollano, 2013).

The Rag-Ragulator Complex Promotes CNS Myelination by Repressing TFEB

Recent work has shown that active Rag GTPases repress TFEB by binding and recruiting it to lysosomes, where TFEB is phosphorylated and inactivated (Martina and Puertollano, 2013). Previous studies show that both *Rraga* and *Tfeb* are expressed in oligodendrocytes and that their expression increases as myelination progresses, consistent with the possibility that RagA antagonizes TFEB activity in oligodendrocytes (Lister et al., 2011; Marques et al., 2016). These previous studies, together with the upregulation of TFEB target genes in myelinating glia of *rraga*$^{-/-}$ mutants, led us to investigate whether aberrantly increased Tfeb activity blocks myelination in *rraga*$^{-/-}$ mutant oligodendrocytes. This hypothesis predicts that Tfeb represses myelination and that inactivation of Tfeb would rescue CNS myelination in *rraga*$^{-/-}$ mutants (Figure 3B).

We used CRISPR-Cas9 to generate mutations near the 5′ end of the *tfeb* coding sequence and established two new alleles of *tfeb*: *tfeb*^{st120} and *tfeb*^{st121} (Figure 3C). As expected for a loss-of-function allele, quantitative RT-PCR analysis showed that some known TFEB target genes are indeed downregulated in *tfeb* transheterozygous mutants (*tfeb*$^{st120/st121}$, henceforth indicated as *tfeb*$^{-/-}$ mutant), including *hexa*, *gba*, *gla*, *neu1, psap*, *and sqstm1* (Figure S4B). Strikingly, expression of *mbp* and *plp1b* mRNA was partially restored in *rraga*$^{-/-}$ mutants heterozygous for *tfeb*$^{+/-}$ mutations, and *mbp* was restored to wild-type levels in *rraga*$^{-/-}$;*tfeb*$^{-/-}$ double mutants (Figures 3D and S5). Furthermore, in the ventral spinal cord, electron microscopy analysis revealed that *rraga*$^{-/-}$; *tfeb*$^{-/-}$ double mutants have many more myelinated axons than *rraga*$^{-/-}$ single mutants (36 and 8, respectively) (Figures 3E and 3F). Our analysis of myelin gene expression and myelin ultrastructure in these mutants indicates that Tfeb is hyperactive in oligodendrocytes of *rraga*$^{-/-}$ mutants and that inhibiting Tfeb activity can rescue myelination in *rraga*$^{-/-}$ mutants.

To test the hypothesis that Tfeb represses myelination in the developing CNS, we examined expression of *mbp* mRNA, myelin ultrastructure, and MBP protein in *tfeb*$^{-/-}$ mutant larvae. At 5 dpf, *mbp* and *plp1b* mRNA levels are indistinguishable in *tfeb*$^{-/-}$ mutants and their wild-type siblings (Figures 3D and S5). To determine if *tfeb*$^{-/-}$ mutants have normal myelin, we next examined CNS ultrastructure by transmission electron microscopy. While our analysis revealed no statistical difference

(D) Lateral view of 4 dpf *Tg(olig2:EGFP)* larvae showing comparable numbers of *olig2*-positive cells in both the wild-type (top panel) and *rraga*$^{-/-}$ mutant (lower panel); panel shows anterior to the left and dorsal up. See also Figure S2.

(E) Dorsal view of 4-dpf *Tg(claudink:EGFP)* embryos showing presence of oligodendrocytes (arrows) in both wild-type (top panel) and *rraga*$^{-/-}$ mutants (lower panel) but reduced expression of GFP along myelinated axonal tracts (arrowheads). Panel shows anterior to the left and dorsal up. Genotypes of all animals shown were determined by PCR after imaging.

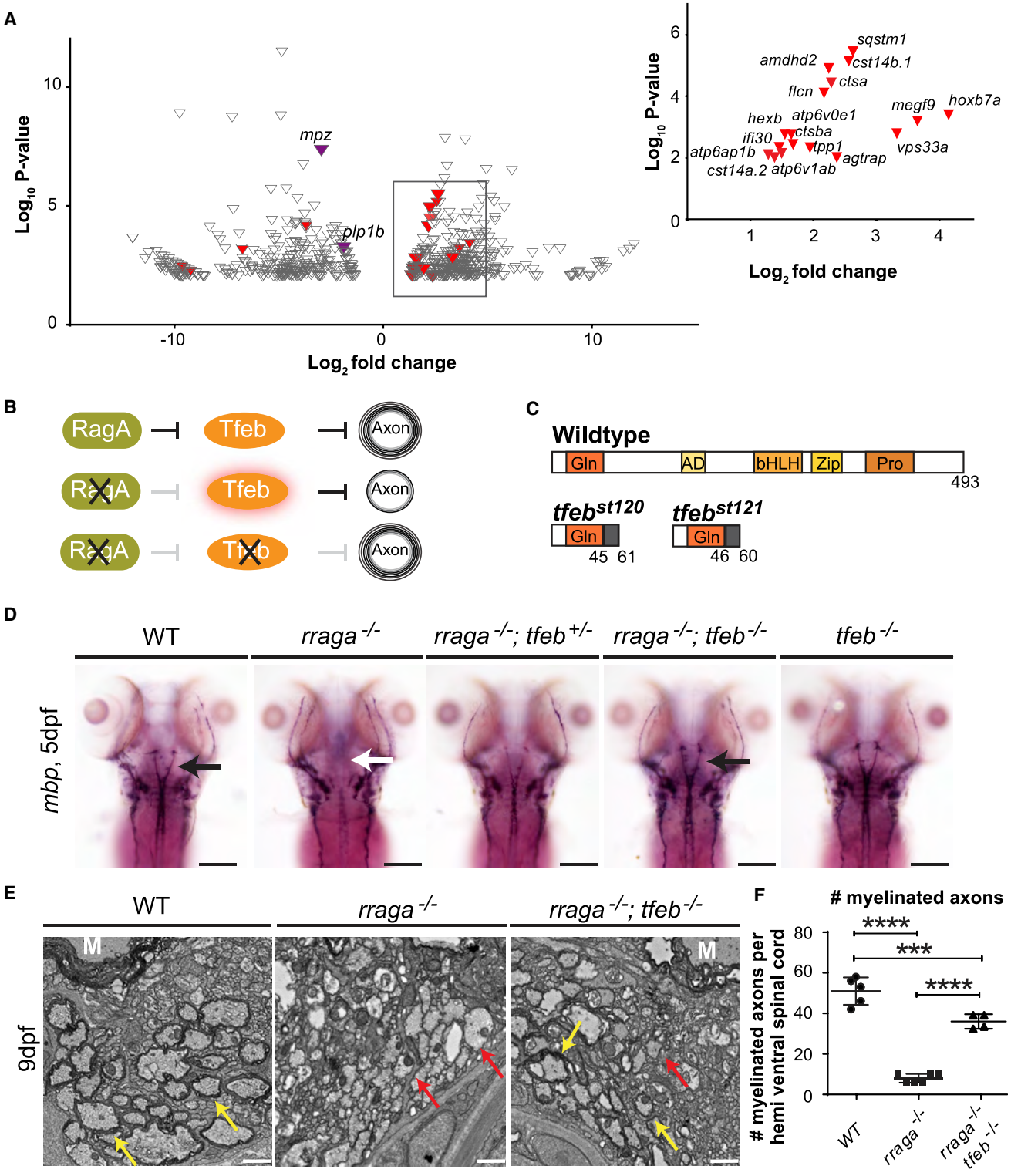


Figure 3. RagA Promotes CNS Myelination by Repressing Tfeb

(A) Volcano plot depicting the genes differentially expressed ($p < 0.01$) in *rraga*$^{-/-}$ mutants relative to wild-type animals. Among the significantly downregulated genes (< 2.5×) are *mpz* and *plp1b* (purple), which at this stage are characteristic of CNS myelin. Expression levels of 17 previously defined targets of TFEB (red) are upregulated (> 2.5) in *rraga*$^{-/-}$ mutants. Inset graph depicts previously known TFEB targets (red) upregulated in *rraga*$^{-/-}$ mutants. See also Tables S1, S2, and S3.

(B) Diagrammatic representation of the hypothesis that RagA promotes myelination by repressing Tfeb, which inhibits CNS myelination.

(legend continued on next page)

in the number of myelinated axons in the ventral spinal cord of *tfeb*$^{-/-}$ mutants and their wild-type siblings (ventral: 54 versus 51; Figure 4A), there was a significant increase in the number of myelinated axons in the dorsal spinal cord of *tfeb*$^{-/-}$ mutants (dorsal: 48 versus 32; Figure 4B). To determine if oligodendrocytes are altered in the brain of *tfeb*$^{-/-}$ mutants, we examined the expression and localization of MBP protein in the hindbrain of 8-dpf *tfeb*$^{-/-}$ mutants and siblings. MBP protein is normally localized in oligodendrocyte processes and largely excluded from the cell body (Figure 4C). In the hindbrain of 8-dpf *tfeb*$^{-/-}$ mutants, however, we observed MBP ectopically expressed in a region of the hindbrain that normally contains oligodendrocyte cell bodies with little or no MBP (Figures 4C and 4D, red arrows). Our analysis of *tfeb*$^{-/-}$ and *rraga*$^{-/-}$;*tfeb*$^{-/-}$ double mutants indicates that Tfeb represses myelination in CNS and that RagA is essential to prevent hyperactivity of Tfeb in oligodendrocytes.

Our hypothesis that TFEB activity represses myelination in the CNS predicts that overexpression of a constitutively active (i.e., nonphosphorylatable) form of Tfeb will repress myelination (Puertollano et al., 2018; Sardiello et al., 2009; Settembre et al., 2011). To determine if overexpression of constitutively active Tfeb represses myelination, we transiently expressed a phosphorylation-null Tfeb mutant (Tfeb PN: S3A+S149A+S221A+S484A+S486A) under the control of the *claudink* promoter. Transient transgenesis results in high variability of transgene expression both within and between individuals. To select individuals with a higher rate of transgenesis, the transgenesis vector contained a *cmlc2:*GFP reporter, which allowed transgenic animals to be identified by GFP expression in the heart. At 4 dpf, injected fish were sorted into GFP+ or GFP− groups (transgenic and weakly or non-transgenic, respectively), and *mbp* expression was monitored by ISH. As predicted, transient overexpression of phosphorylation-null Tfeb resulted in a decrease in *mbp* mRNA expression levels in some of the injected fish (Phospho-null 12%, 6/50 fish) (Figure 4E). Together, our data provide evidence that RagA functions to promote myelination by repressing TFEB, which in turn inhibits myelination in the CNS.

Levels of Cytoplasmic TFEB Increase in Remyelinating Lesions in Mouse

Our data indicate that Tfeb represses myelination during development. We next explored whether TFEB is altered after injury during the process of remyelination. We used an adult mouse model of demyelination and remyelination, where focal demyelination is induced by stereotactic injection of the demyelinating agent L-α-lysophosphatidylcholine (LPC) into the *corpus callosum* (Boyd et al., 2013) (Figure 5A). Remyelination relies on the recruitment of OPCs to demyelinated lesions and their subsequent differentiation into myelin-forming oligodendrocytes. In this model, oligodendrocyte differentiation begins at 10 days post injection (dpi), early remyelination is present at 14 dpi and is complete by 28 dpi (Boyd et al., 2013). Immunohistochemical analysis of control adult mouse *corpus callosum* (either uninjected or injected with PBS) showed that the majority of CC1+ oligodendrocytes have low levels of cytoplasmic TFEB expression, but there were a small number of oligodendrocytes with high TFEB expression (Figures 5B–5D). TFEB expression was almost exclusively localized to the cytoplasm of CC1+ oligodendrocytes, with nuclear TFEB localization rarely observed (approximately 1/cell per optical frame) (Figures 5B–5D). During the early stages of remyelination (14 dpi), we observed a significant increase in the number of oligodendrocytes with high cytoplasmic TFEB expression in the lesion and perilesion areas (Figures 5E and 5E′). The number of oligodendrocytes with high cytoplasmic expression of TFEB dropped significantly at the late remyelination stage (28 dpi), when the lesion is mostly remyelinated (Figures 5F and F′).

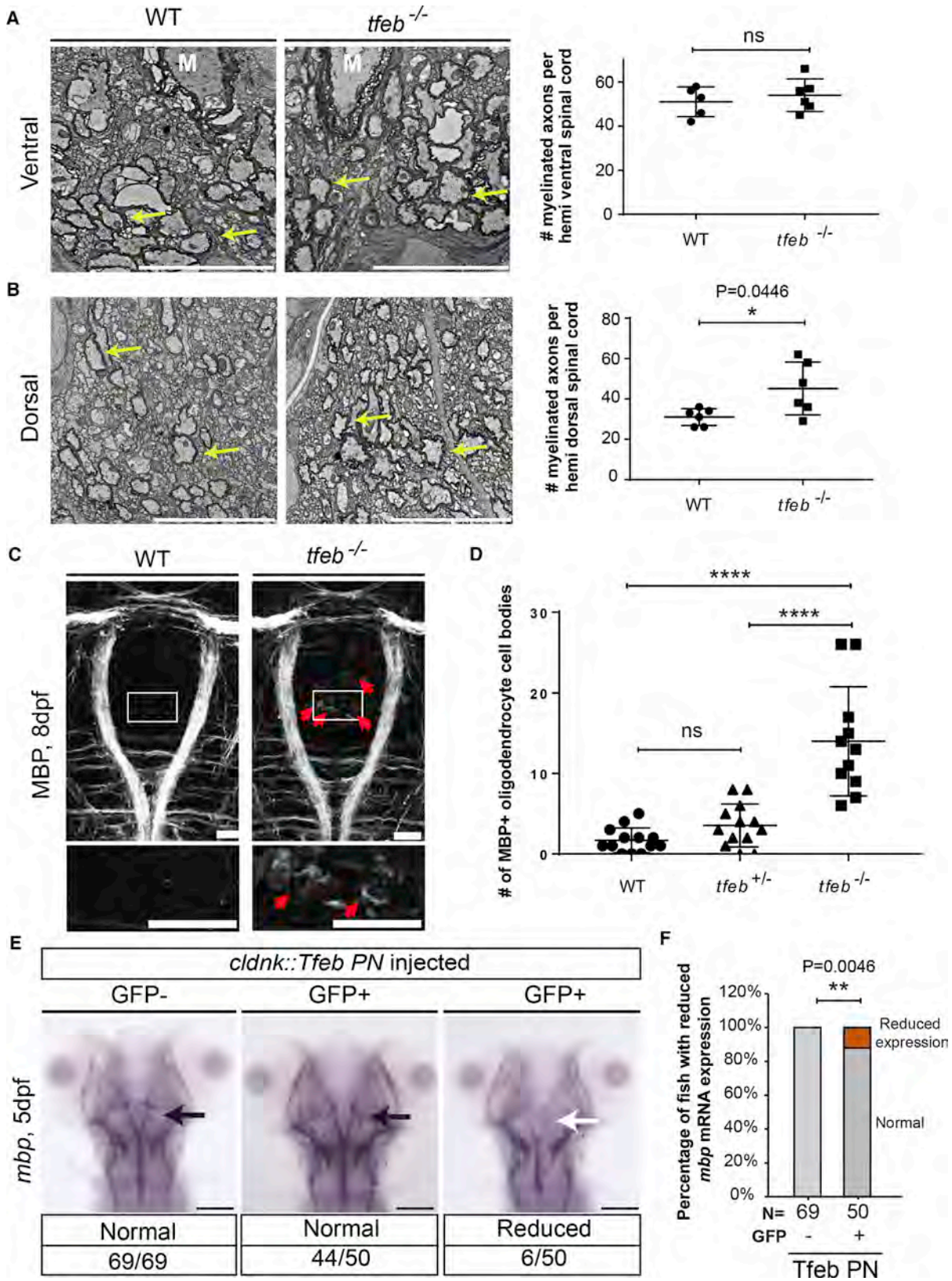
DISCUSSION

TFEB Represses Myelination

Our experiments demonstrate that TFEB inhibits myelination. Tfeb loss-of-function mutations cause ectopic myelination in the dorsal spinal cord and ectopic expression of MBP in the hindbrain. Conversely, *rraga*$^{-/-}$ mutants have increased Tfeb activity, which in turn blocks myelination. Furthermore, expression of constitutively active Tfeb also inhibits *mbp* expression. Consistent with previous biochemical studies (Martina and Puertollano, 2013), our analyses showed that RagA and Tfeb have opposing functions in CNS myelination *in vivo*. In striking contrast to *rraga*$^{-/-}$ single mutants, *rraga*$^{-/-}$; *tfeb*$^{-/-}$ double mutants have apparently normal levels of *mbp* expression. Expression of *mbp* is also partially rescued in *rraga*$^{-/-}$; *tfeb*$^{+/-}$ mutants, indicating that myelination is very sensitive to the level of *tfeb* function. Thus, the analysis of both loss and gain of Tfeb activity defines Tfeb as a repressor of myelination.

Oligodendrocytes are present in *rraga*$^{-/-}$ mutants and are competent to myelinate if *tfeb* activity is partially (haploinsufficiency) or fully eliminated, indicating that Tfeb blocks *mbp* expression in pre-myelinating oligodendrocytes. Previous studies have defined a brief developmental window (~5 hr in zebrafish) during which an oligodendrocyte can initiate new myelin segments (Czopka et al., 2013). After this critical period,new myelin segments are not initiated, although previously established segments are maintained and expanded. It is possible that Tfeb closes the critical period, such that myelination is greatly curtailed by hyperactive Tfeb in *rraga*$^{-/-}$ mutants.

(C) Diagrammatic representation of Tfeb protein and of predicted truncated proteins encoded by *tfeb*^{st120} and *tfeb*^{st121} mutant alleles.
(D) Expression of *mbp* mRNA, as detected by whole mount in situ hybridization, is reduced in CNS of *rraga*$^{-/-}$ mutants, but is restored in *rraga*$^{-/-}$;*tfeb*$^{-/-}$ double mutants. *rraga*$^{-/-}$;*tfeb*$^{-/-}$ double mutants and *tfeb*$^{-/-}$ mutants are indistinguishable from wild-type larvae. See also Figure S5. Scale bar, 50 μm.
(E) TEM images of transverse sections of the ventral spinal cord (CNS) at 9 dpf show that myelination is restored in *rraga*$^{-/-}$;*tfeb*$^{-/-}$ double mutants. Red arrows indicate unmyelinated axons, and yellow arrows indicate myelinated axons. Scale bar, 1μm.
(F) Quantification of the number of myelinated axons per hemi ventral spinal cord at 9 dpf is shown on the right; graph depicts average values and standard deviation; individual measurements are also shown. 3 individuals of each genotype were analyzed. (Statistical analysis: pairwise comparisons using one-way ANOVA; Tukey post hoc test significant interaction ****$p < 0.0001$, ***$p < 0.001$).



(legend on next page)

There are many possible mechanisms by which TFEB might repress myelination. TFEB is a transcriptional regulatory protein, raising the possibility that TFEB might directly repress myelin gene expression in oligodendrocytes. There are, however, no reported TFEB binding sites in the vicinity of the *mbp* gene, suggesting that TFEB represses myelination indirectly. In other cell types, TFEB activates hundreds of target genes that regulate diverse lysosome-related processes, including lysosome biogenesis and exocytosis, autophagy, and lipid catabolism (Napolitano and Ballabio, 2016). Our analysis indicates that TFEB activates at least some of these previously known target genes in oligodendrocytes as well. It is likely that inappropriately increased activity of one or more TFEB-regulated processes disrupts myelination in oligodendrocytes. For example, TFEB hyperactivity might disrupt the trafficking of endolysosomal organelles to the membrane or synthesis of lipids critical for the formation of the membranous myelin sheath, which could in turn impede myelination.

RagA and Other Regulators of TFEB in Myelination

Our mutational analysis demonstrates that the lysosomal genes *rraga* and *lamtor4* are essential for myelination in the CNS, but not the PNS. RagA and Lamtor4 are components of the Rag-Ragulator complex, which recruits TFEB to the lysosome, where it is phosphorylated and inactivated (Efeyan et al., 2015). mTOR, which is recruited to the lysosome by RagA-dependent and -independent mechanisms, is one kinase that can phosphorylate and inactivate TFEB (Martina et al., 2012; Roczniak-Ferguson et al., 2012; Settembre et al., 2011, 2012). If mTOR inactivated Tfeb in the context of myelination, we would expect $mtor^{-/-}$ mutants to have hyperactive Tfeb and a phenotype similar to $rraga^{-/-}$ mutants. Our data, however, suggest that mTOR is not the only kinase that can repress Tfeb activity in oligodendrocytes because $mtor^{-/-}$ mutants have much more *mbp* expression in oligodendrocytes than $rraga^{-/-}$ mutants. Previous studies show that the kinases GSKβ3, ERK2, AKT, and PKCβ can also phosphorylate TFEB, and some combination of these likely controls TFEB activity during myelination (Li et al., 2016; Martina and Puertollano, 2013; Medina et al., 2015; Palmieri et al., 2017; Puertollano et al., 2018; Roczniak-Ferguson et al., 2012; Settembre et al., 2011).

TFEB during Remyelination

Our analysis indicates that Tfeb represses myelination during development, raising the question of its role during remyelination. In control mouse white matter, TFEB is mainly detected at low levels in the cytoplasm of mature oligodendrocytes and is rarely localized in the nucleus. TFEB protein levels increase in the cytoplasm of mature oligodendrocytes during remyelination, suggesting that it is predominantly inactive and thus permitting the remyelination process. After remyelination is complete, TFEB expression declined to near normal levels. It may seem somewhat paradoxical that levels of TFEB—a repressor of myelination—increase in remyelinating cells. One possibility is that TFEB, as a component of the integrated stress response (Martina et al., 2016), is more highly expressed due to the stress of the injury and is subsequently inactivated by cytoplasmic localization when remyelination commences. RagA and kinases that phosphorylate TFEB (GSKβ3, ERK2, AKT, PKCβ, mTORC) may be essential to retain TFEB in the cytoplasm during remyelination. Animals with increased TFEB function, e.g., $rraga^{-/-}$ mutants or Tfeb phosphorylation-null transgenic animals, will be valuable models in which to better characterize the role of TFEB and its regulators in the context of remyelination.

Understanding the nature of the signals that regulate TFEB expression and localization in oligodendrocytes of the healthy and diseased brain will be critical to understanding its function in oligodendrocyte development, myelination, and remyelination. Elucidating the target genes and processes downstream of TFEB that are inhibitory to myelination may define additional regulators of myelination and myelin repair, which in turn may suggest strategies for therapeutic remyelination.

STAR★METHODS

Detailed methods are provided in the online version of this paper and include the following:

- KEY RESOURCES TABLE
- CONTACT FOR REAGENT AND RESOURCE SHARING
- EXPERIMENTAL MODEL AND SUBJECT DETAILS
  - Zebrafish
  - Mouse
- METHOD DETAILS
  - *In Situ* Hybridization
  - Whole-Mount Immunofluorescence
  - Crispr/Cas9 Targeting
  - FAC Sorting and RNA Sequencing
  - qRT-PCR
  - RNA-Seq Analysis
  - Gene Ontology Enrichment

Figure 4. TFEB Represses Myelination in the CNS

(A and B) TEM images of transverse sections of the spinal cord at 9 dpf show an increased number of myelinated axons in the dorsal spinal cord of *tfeb* mutants. Quantification of the number of myelinated axons per ventral (A) or dorsal (B) hemi spinal cord is shown on the right. Graph depicts average values and standard deviation; individual measurements are also shown. Yellow arrows indicate myelinated axons. Scale bar, 5 μm. (Statistical analysis: two-tailed unpaired t test with Welch's correction). 3 wild-type and 4 $tfeb^{-/-}$ mutant animals were analyzed.

(C) Dorsal view of the hindbrain of 8-dpf larvae shows robust expression of MBP protein in myelinating oligodendrocyte processes in wild-type and $tfeb^{-/-}$ mutants and ectopic expression of MBP protein in $tfeb^{-/-}$ mutant cell bodies (red arrows). Scale bar, 50 μm.

(D) Quantification of the number of ectopic MBP-positive cells in $tfeb^{-/-}$ mutants ($tfeb^{-/-}$; n = 11) and siblings (n = 13 for wild-type and $tfeb^{+/-}$ heterozygotes) (Pairwise comparisons using one-way ANOVA; Tukey post hoc test significant interaction; ****p < 0.0001); bars represent standard deviation values. Individual values are also depicted. Genotypes of all animals shown were determined by PCR after imaging.

(E) Whole mount in situ hybridization analysis of *mbp* mRNA expression in 5-dpf fish following transgenic expression of phosphorylation-null Tfeb (Tfeb NP) under the control of *claudink* promoter. *mbp* mRNA expression is reduced in some fish overexpressing the construct.

(F) Quantification of the percentage of fish with reduced *mbp* mRNA expression. (Statistical analysis: Fisher's exact test, two-tailed, **p < 0.01).

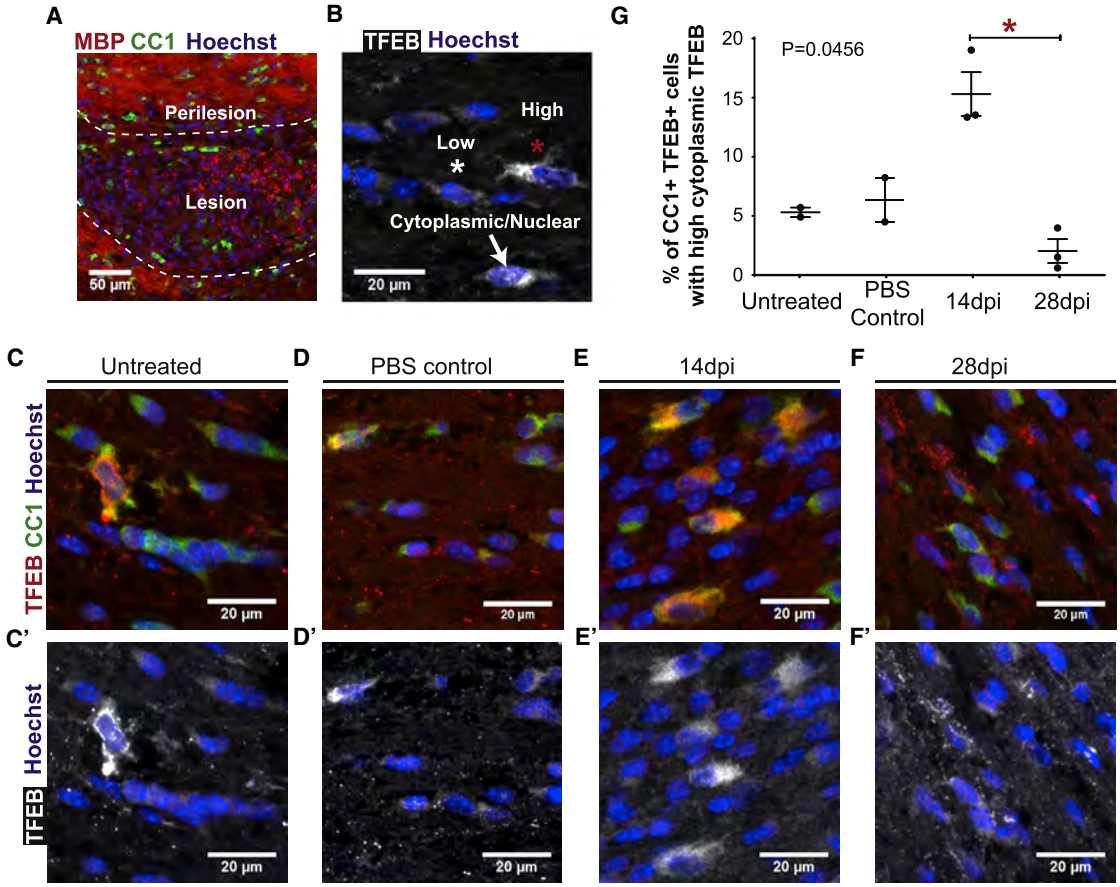


Figure 5. Remyelinating Lesions in Mouse Show Increased Levels of Cytoplasmic TFEB

(A) Low-power image of LPC-injected *corpus callosum* 14 dpi, stained for MBP (red), CC1 (green), and Hoechst (blue). The area of the lesion is outlined with dashed white line, and the perilesion area is marked.

(B) High-power image of control *corpus callosum* stained for TFEB (white) and Hoechst (blue). TFEB is mostly found in the cytoplasm in mature oligodendrocytes of the rodent *corpus callosum*, both in those expressing low levels (white asterisk) and high levels (red asterisk). Rarely, both cytoplasmic and nuclear TFEB expression is detected (white arrow).

(C) High-power image of adult, untreated, control *corpus callosum* stained for TFEB (red), CC1 (green), and Hoechst (blue). (C') Single channel of TFEB staining (white) and Hoechst (blue). A few mature, CC1 (green)-expressing oligodendrocytes of the adult, normal rodent *corpus callosum* show high level expression of TFEB (red) in the cytoplasm. Most express low levels of TFEB in the cytoplasm (C′; TFEB white).

(D) High-power image of adult, PBS-injected control *corpus callosum* 14 dpi stained for TFEB (red), CC1 (green), and Hoechst (blue). (D') Single channel of TFEB staining (white) and Hoechst (blue). CC1+ oligodendrocytes display a similar TFEB expression profile to untreated controls (C and C').

(E) High-power image of adult, LPC-injected tissue 14 dpi (early remyelination time point) stained for TFEB (red), CC1 (green), and Hoechst (blue). (E') Single channel of TFEB staining (white) and Hoechst (blue). An increased number of CC1+ oligodendrocytes with high cytoplasmic TFEB expression appears in the *corpus callosum*.

(F) High-power image of adult, LPC-injected tissue 28 dpi (late remyelination time point) stained for TFEB (red), CC1 (green), and Hoechst (blue). (F') Single channel of TFEB staining (white) and Hoechst (blue). Very few CC1+ oligodendrocytes have high cytoplasmic TFEB expression.

(G) Quantification of the percentage of CC1+TFEB+ cells with high cytoplasmic TFEB levels in the *corpus callosum* after LPC focal lesion induction. Graph depicts average value and SEM. Individuals values are also represented. A marked increase is observed during early remyelination in lesion and perilesion areas (14 dpi) that significantly drops at later remyelination stages. Statistical analysis: non-parametric ANOVA (Kruskal-Wallis test) with Dunn's post hoc test. Total p value, 0.0456; and significance between 14 dpi and 28 dpi.

- Identification of Tfeb Targets in Genes Upregulated in *rraga*$^{-/-}$ Mutants
- Expression Constructs and Transient Injections
- Transmission Electron Microscopy
- Drug Treatment
- LPC-Induced Demyelinating Lesions in Rodents
- Immunohistochemistry of Mouse Tissue and Quantification

● QUANTIFICATION AND STATISTICAL ANALYSIS

SUPPLEMENTAL INFORMATION

Supplemental Information includes five figures and three tables and can be found with this article online at https://doi.org/10.1016/j.devcel.2018.10.003.

ACKNOWLEDGMENTS

We thank Talbot laboratory members for helpful discussions and technical advice and Tuky K. Reyes and Chenelle Hill for fish maintenance. Transmission electron microscopy was performed with assistance from John J. Perrino in

the Stanford Cell Sciences Imaging Facility; this work was supported in part by ARRA Award number 1S10RR026780-01 from the National Center for Research Resources (NCRR). Cell sorting for this project was performed with assistance from Brandon J. Carter and Qianyi Lee, using instruments in the Stanford Shared FACS Facility. RNA sequencing was performed with assistance from the Stanford Functional Genomics Facility. Mouse tissue was kindly generated by Amanda Boyd. K.S. was supported by a fellowship from A*STAR Singapore, and E.L.B. was supported by a fellowship from the National Science Foundation. W.S.T. is a Catherine R. Kennedy and Daniel L. Grossman Fellow in Human Biology. L.Z. and A.W. are supported by an MS Society UK Centre Grant. This work was supported by NIH grant R01NS050223 and NMSS grant RG-1707-28694 to W.S.T.

AUTHOR CONTRIBUTIONS

K.S. and W.S.T. formulated the idea. K.S. and A.M.M. designed, performed, and analyzed the experiments on zebrafish. K.S. and H.I. performed and analyzed quantitative PCR analysis. K.S., H.I., and E.L.B. performed bioinformatics analysis. L.Z. and A.W. designed, performed, and analyzed experiments pertaining to mice. A.M.M., K.S., H.I., and W.S.T. analyzed data and wrote the manuscript with input from all authors.

DECLARATION OF INTERESTS

The authors declare no competing interests.

Received: March 28, 2018
Revised: August 28, 2018
Accepted: October 3, 2018
Published: November 5, 2018

REFERENCES

Almeida, R.G., and Lyons, D.A. (2017). On myelinated axon plasticity and neuronal circuit formation and function. J. Neurosci. *37*, 10023–10034.

Appelqvist, H., Wäster, P., Kågedal, K., and Öllinger, K. (2013). The lysosome: from waste bag to potential therapeutic target. J. Mol. Cell Biol. *5*, 214–226.

Bar-Peled, L., Schweitzer, L.D., Zoncu, R., and Sabatini, D.M. (2012). Ragulator is a GEF for the rag GTPases that signal amino acid levels to mTORC1. Cell *150*, 1196–1208.

Bengtsson, S.L., Nagy, Z., Skare, S., Forsman, L., Forssberg, H., and Ullén, F. (2005). Extensive piano practicing has regionally specific effects on white matter development. Nat. Neurosci. *8*, 1148–1150.

Boyd, A., Zhang, H., and Williams, A. (2013). Insufficient OPC migration into demyelinated lesions is a cause of poor remyelination in MS and mouse models. Acta Neuropathol. *125*, 841–859.

Browne, P., Chandraratna, D., Angood, C., Tremlett, H., Baker, C., Taylor, B.V., and Thompson, A.J. (2014). Atlas of multiple sclerosis 2013: a growing global problem with widespread inequity. Neurology *83*, 1022–1024.

Czopka, T., Ffrench-Constant, C., and Lyons, D.A. (2013). Individual oligodendrocytes have only a few hours in which to generate new myelin sheaths in vivo. Dev. Cell *25*, 599–609.

Ding, Y., Sun, X., Huang, W., Hoage, T., Redfield, M., Kushwaha, S., Sivasubbu, S., Lin, X., Ekker, S., and Xu, X. (2011). Haploinsufficiency of target of rapamycin attenuates cardiomyopathies in adult ZebrafishNovelty and significance. Circ. Res. *109*, 658–669.

Dutta, R., and Trapp, B.D. (2011). Mechanisms of neuronal dysfunction and degeneration in multiple sclerosis. Prog. Neurobiol. *93*, 1–12.

Efeyan, A., Comb, W.C., and Sabatini, D.M. (2015). Nutrient-sensing mechanisms and pathways. Nature *517*, 302–310.

Emery, B. (2010). Regulation of oligodendrocyte differentiation and myelination. Science *330*, 779–782.

Ferguson, S.M. (2015). Beyond indigestion: emerging roles for lysosome-based signaling in human disease. Curr. Opin. Cell Biol. *35*, 59–68.

Franklin, R.J.M., and Ffrench-Constant, C. (2008). Remyelination in the CNS: from biology to therapy. Nat. Rev. Neurosci. *9*, 839–855.

Fünfschilling, U., Supplie, L.M., Mahad, D., Boretius, S., Saab, A.S., Edgar, J., Brinkmann, B.G., Kassmann, C.M., Tzvetanova, I.D., Möbius, W., et al. (2012). Glycolytic oligodendrocytes maintain myelin and long-term axonal integrity. Nature *485*, 517–521.

Kim, E., Goraksha-Hicks, P., Li, L., Neufeld, T.P., and Guan, K.L. (2008). Regulation of TORC1 by Rag GTPases in nutrient response. Nat. Cell Biol. *10*, 935–945.

Kim, Y.C., Park, H.W., Sciarretta, S., Mo, J.S., Jewell, J.L., Russell, R.C., Wu, X., Sadoshima, J., and Guan, K.L. (2014). Rag GTPases are cardioprotective by regulating lysosomal function. Nat. Commun. *5*, 4241.

Labun, K., Montague, T.G., Gagnon, J.A., Thyme, S.B., and Valen, E. (2016). CHOPCHOP v2: a web tool for the next generation of CRISPR genome engineering. Nucleic Acids Res. *44*, W272–W276.

Li, Y., Xu, M., Ding, X., Yan, C., Song, Z., Chen, L., Huang, X., Wang, X., Jian, Y., Tang, G., et al. (2016). Protein kinase C controls lysosome biogenesis independently of mTORC1. Nat. Cell Biol. *18*, 1065–1077.

Lister, J.A., Lane, B.M., Nguyen, A., and Lunney, K. (2011). Embryonic expression of zebrafish MiT family genes tfe3b, tfeb, and tfec. Dev. Dyn. *240*, 2529–2538.

Lyons, D.A., Pogoda, H.M., Voas, M.G., Woods, I.G., Diamond, B., Nix, R., Arana, N., Jacobs, J., and Talbot, W.S. (2005). erbb3 and erbb2 are essential for Schwann cell migration and myelination in zebrafish. Curr. Biol. *15*, 513–524.

Lyons, D.A., Naylor, S.G., Mercurio, S., Dominguez, C., and Talbot, W.S. (2008). KBP is essential for axonal structure, outgrowth and maintenance in zebrafish, providing insight into the cellular basis of Goldberg-Shprintzen syndrome. Development *135*, 599–608.

Lyons, D.A., Naylor, S.G., Scholze, A., and Talbot, W.S. (2009). Kif1b is essential for mRNA localization in oligodendrocytes and development of myelinated axons. Nat. Genet. *41*, 854–858.

Manoli, M., and Driever, W. (2012). Fluorescence-activated cell sorting (FACS) of fluorescently tagged cells from zebrafish larvae for RNA isolation. Cold Spring Harb. Protoc. *2012*, 879–886.

Marques, S., Zeisel, A., Codeluppi, S., van Bruggen, D., Mendanha Falcão, A., Xiao, L., Li, H., Häring, M., Hochgerner, H., Romanov, R.A., et al. (2016). Oligodendrocyte heterogeneity in the mouse juvenile and adult central nervous system. Science *352*, 1326–1329.

Martina, J.A., and Puertollano, R. (2013). Rag GTPases mediate amino acid-dependent recruitment of TFEB and MITF to lysosomes. J. Cell Biol. *200*, 475–491.

Martina, J.A., Chen, Y., Gucek, M., and Puertollano, R. (2012). MTORC1 functions as a transcriptional regulator of autophagy by preventing nuclear transport of TFEB. Autophagy *8*, 903–914.

Martina, J.A., Diab, H.I., Brady, O.A., and Puertollano, R. (2016). TFEB and TFE3 are novel components of the integrated stress response. EMBO J. *35*, 479–495.

Martini-Stoica, H., Xu, Y., Ballabio, A., and Zheng, H. (2016). The autophagy-lysosomal pathway in neurodegeneration: a TFEB perspective. Trends Neurosci. *39*, 221–234.

McKenzie, I.A., Ohayon, D., Li, H., de Faria, J.P., Emery, B., Tohyama, K., and Richardson, W.D. (2014). Motor skill learning requires active central myelination. Science *346*, 318–322.

Medina, D.L., Fraldi, A., Bouche, V., Annunziata, F., Mansueto, G., Spampanato, C., Puri, C., Pignata, A., Martina, J.A., Sardiello, M., et al. (2011). Transcriptional activation of lysosomal exocytosis promotes cellular clearance. Dev. Cell *21*, 421–430.

Medina, D.L., Di Paola, S., Peluso, I., Armani, A., De Stefani, D., Venditti, R., Montefusco, S., Scotto-Rosato, A., Prezioso, C., Forrester, A., et al. (2015). Lysosomal calcium signalling regulates autophagy through calcineurin and TFEB. Nat. Cell Biol. *17*, 288–299.

Mi, H., Muruganujan, A., Casagrande, J.T., and Thomas, P.D. (2013). Large-scale gene function analysis with the PANTHER classification system. Nat. Protoc. *8*, 1551–1566.

Mi, H., Huang, X., Muruganujan, A., Tang, H., Mills, C., Kang, D., and Thomas, P.D. (2017). PANTHER version 11: expanded annotation data from Gene Ontology and Reactome pathways, and data analysis tool enhancements. Nucleic Acids Res. *45*, D183–D189.

Montague, T.G., Cruz, J.M., Gagnon, J.A., Church, G.M., and Valen, E. (2014). CHOPCHOP: a CRISPR/Cas9 and TALEN web tool for genome editing. Nucleic Acids Res. *42*, W401–W407.

Münzel, E.J., Schaefer, K., Obirei, B., Kremmer, E., Burton, E.A., Kuscha, V., Becker, C.G., Brösamle, C., Williams, A., and Becker, T. (2012). Claudin k is specifically expressed in cells that form myelin during development of the nervous system and regeneration of the optic nerve in adult zebrafish. Glia *60*, 253–270.

Münzel, E.J., and Williams, A. (2013). Promoting remyelination in multiple sclerosis-recent advances. Drugs *73*, 2017–2029.

Napolitano, G., and Ballabio, A. (2016). TFEB at a glance. J. Cell Sci. *129*, 2475–2481.

Nezich, C.L., Wang, C., Fogel, A.I., and Youle, R.J. (2015). MiT/TFE transcription factors are activated during mitophagy downstream of Parkin and Atg5. J. Cell Biol. *210*, 435–450.

Palmieri, M., Impey, S., Kang, H., di Ronza, A., Pelz, C., Sardiello, M., and Ballabio, A. (2011). Characterization of the CLEAR network reveals an integrated control of cellular clearance pathways. Hum. Mol. Genet. *20*, 3852–3866.

Palmieri, M., Pal, R., Nelvagal, H.R., Lotfi, P., Stinnett, G.R., Seymour, M.L., Chaudhury, A., Bajaj, L., Bondar, V.V., Bremner, L., et al. (2017). mTORC1-independent TFEB activation via Akt inhibition promotes cellular clearance in neurodegenerative storage diseases. Nat. Commun. *8*, 14338.

Park, H.C., Mehta, A., Richardson, J.S., and Appel, B. (2002). olig2 is required for zebrafish primary motor neuron and oligodendrocyte development. Dev. Biol. *248*, 356–368.

Puertollano, R., Ferguson, S.M., Brugarolas, J., and Ballabio, A. (2018). The complex relationship between TFEB transcription factor phosphorylation and subcellular localization. EMBO J. *37*, e98804.

Ravanelli, A.M., and Appel, B. (2015). Motor neurons and oligodendrocytes arise from distinct cell lineages by progenitor recruitment. Genes Dev. *29*, 2504–2515.

Roczniak-Ferguson, A., Petit, C.S., Froehlich, F., Qian, S., Ky, J., Angarola, B., Walther, T.C., and Ferguson, S.M. (2012). The transcription factor TFEB links mTORC1 signaling to transcriptional control of lysosome homeostasis. Sci. Signal. *5*, ra42.

Saftig, P., and Haas, A. (2016). Turn up the lysosome. Nat. Cell Biol. *18*, 1025–1027.

Sancak, Y., Peterson, T.R., Shaul, Y.D., Lindquist, R.A., Thoreen, C.C., Bar-Peled, L., and Sabatini, D.M. (2008). The rag GTPases bind raptor and mediate amino acid signaling to mTORC1. Science *320*, 1496–1501.

Sancak, Y., Bar-Peled, L., Zoncu, R., Markhard, A.L., Nada, S., and Sabatini, D.M. (2010). Ragulator-rag complex targets mTORC1 to the lysosomal surface and is necessary for its activation by amino acids. Cell *141*, 290–303.

Sardiello, M. (2016). Transcription factor EB: from master coordinator of lysosomal pathways to candidate therapeutic target in degenerative storage diseases. Ann. N. Y. Acad. Sci. *1371*, 3–14.

Sardiello, M., Palmieri, M., di Ronza, A., Medina, D.L., Valenza, M., Gennarino, V.A., Di Malta, C.D., Donaudy, F., Embrione, V., Polishchuk, R.S., et al. (2009). A gene network regulating lysosomal biogenesis and function. Science *325*, 473–477.

Settembre, C., and Ballabio, A. (2014). Lysosomal adaptation: how the lysosome responds to external cues. Cold Spring Harb. Perspect. Biol. *6*, a016907.

Settembre, C., Di Malta, C., Polito, V.A., Garcia Arencibia, M., Vetrini, F., Erdin, S., Erdin, S.U., Huynh, T., Medina, D., Colella, P., et al. (2011). TFEB links autophagy to lysosomal biogenesis. Science *332*, 1429–1433.

Settembre, C., Zoncu, R., Medina, D.L., Vetrini, F., Erdin, S., Erdin, S., Huynh, T., Ferron, M., Karsenty, G., Vellard, M.C., et al. (2012). A lysosome-to-nucleus signalling mechanism senses and regulates the lysosome via mTOR and TFEB. EMBO J. *31*, 1095–1108.

Settembre, C., Fraldi, A., Medina, D.L., and Ballabio, A. (2013). Signals from the lysosome: a control centre for cellular clearance and energy metabolism. Nat. Rev. Mol. Cell Biol. *14*, 283–296.

Shaw, R.J. (2008). MTOR signaling: RAG GTPases transmit the amino acid signal. Trends Biochem. Sci. *33*, 565–568.

Shen, K., Sidik, H., and Talbot, W.S. (2016). The rag-Ragulator complex regulates lysosome function and phagocytic flux in microglia. Cell Rep. *14*, 547–559.

Sherman, D.L., and Brophy, P.J. (2005). Mechanisms of axon ensheathment and myelin growth. Nat. Rev. Neurosci. *6*, 683–690.

Shiau, C.E., Monk, K.R., Joo, W., and Talbot, W.S. (2013). An anti-inflammatory NOD-like receptor is required for microglia development. Cell Rep. *5*, 1342–1352.

Shin, J., Park, H.C., Topczewska, J.M., Mawdsley, D.J., and Appel, B. (2003). Neural cell fate analysis in zebrafish using olig2 BAC transgenics. Methods Cell Sci. *25*, 7–14.

Simons, M., and Nave, K.A. (2015). Oligodendrocytes: myelination and axonal support. Cold Spring Harb. Perspect. Biol. *8*, a020479.

Thisse, B., Heyer, V., Lux, A., Alunni, V., Degrave, A., Seiliez, I., Kirchner, J., Parkhill, J.P., and Thisse, C. (2004). Spatial and temporal expression of the zebrafish genome by large-scale in situ hybridization screening. Methods Cell Biol. *77*, 505–519.

Thoreen, C.C., Chantranupong, L., Keys, H.R., Wang, T., Gray, N.S., and Sabatini, D.M. (2012). A unifying model for mTORC1-mediated regulation of mRNA translation. Nature *485*, 109–113.

Williams, A., Sarkar, S., Cuddon, P., Ttofi, E.K., Saiki, S., Siddiqi, F.H., Jahreiss, L., Fleming, A., Pask, D., Goldsmith, P., et al. (2008). Novel targets for Huntington's disease in an mTOR-independent autophagy pathway. Nat. Chem. Biol. *4*, 295–305.

Zhou, Q., and Anderson, D.J. (2002). The bHLH transcription factors OLIG2 and OLIG1 couple neuronal and glial subtype specification. Cell *109*, 61–73.

STAR★METHODS

KEY RESOURCES TABLE

REAGENT or RESOURCE	SOURCE	IDENTIFIER
Antibodies		
rabbit anti-MBP	Lyons et al. (2005)	N/A
Anti-Digoxigenin-AP, Fab fragments	Sigma-Aldrich	Cat#11093274910; RRID: AB_514497
monoclonal mouse IgG_{2B} anti-APC	MERCK-Millipore	Clone#CC1, OP80; RRID: AB_2057371
monoclonal IgG_{2A} anti-Myelin Proteolipid Protein	MERCK-Millipore	clone PLPC1, MAB388; RRID: AB_177623
polyclonal rabbit IgG anti -TFEB	Bethyl laboratories	A303-673A; RRID: AB_11204751
Chemicals, Peptides, and Recombinant Proteins		
Torin1	Tocris Bioscience	Cat#4247
Recombinant Cas9-NLS protein	Macrolab, Berkeley	http://qb3.berkeley.edu/macrolab/cas9-nls-purified-protein/
Deposited Data		
Raw and analyzed data RNAseq	This publication	GEO: GSE119332
Experimental Models: Organisms/Strains		
Zebrafish: *mtor*^{xu015}	Ding et al. (2011)	N/A
Zebrafish: *Tg(olig2:GFP)*	Shin et al. (2003)	N/A
Zebrafish: *Tg*(*cldnk:GFP*)	Münzel et al. (2012)	N/A
Zebrafish: *tfeb*^{st120}	This publication	N/A
Zebrafish: *tfeb*^{st121}	This publication	N/A
Zebrafish: *rraga*^{st77}	Shen et al. (2016)	N/A
Oligonucleotides		
plp1b riboprobe Forward: AACAGCCGTGGTTGTGTAAAGC Reverse: TATGTTGGCCAGTGCATTTCCAC	This publication	N/A
st120/st121 genotyping primer Forward: GCTCATGCGGGACCAAATGC Reverse: GGTCACACTAACAAATGTGG	This publication	N/A
st77 genotyping primer Forward: GGTACACAAGATGGACCTGGTT Reverse: GATAATTGAGGCAGATGAAGTCTT	Shen et al. (2016)	N/A
atg9b-F GGCACCATATCAAGAACCTCG atg9b-R CCACAAACAGGAATTGCACAAG	This publication	N/A
clcn7-F TCCACGTTTCCCTCCTATTC clcn7-R AGGAACAGTGTATGGCGTTG	This publication	N/A
ctsa-F ATCAGTGGAGCAAAGCACAG ctsa-R GACCAGCGGGTTATTGAGAT	This publication	N/A
ctsba-F TGTGATCTCAGCCCTTTCAG ctsba-R TATGTCCAGCCGTCCAAGTA	This publication	N/A
ctsd-F AGGCCTATTGGCAGATTCAC ctsd-R GTCCACAATGGCTTCACATC	This publication	N/A
ef1a-F AGGACATCCGTCGTGGTAAT ef1a-R AGAGATCTGCACCAGGGTGGTT	This publication	N/A
gba-F TCAGCAGACCAGCCTAGAAA gba-R ACCGTTTGATCCCAGACTTC	This publication	N/A
gla-F TTCGCAAGACCTGTAACCAC gla-R CATGTCAGGGTCATTCCATC	This publication	N/A
hexa-F GACCCTTCCTTTCCGTATCA hexa-R CCTGGCATGTTCAATCACTC	This publication	N/A
lamp1a-F GACGAGACGACCAACCTGAC lamp1a-R CTGCCTCAAACACAACGCTC	This publication	N/A

(*Continued on next page*)

Continued		
REAGENT or RESOURCE	SOURCE	IDENTIFIER
lamp1b-F TGAACTACTTGGTGGGAACG lamp1b-R ATCTCCCTTGACACCGAAAG	This publication	N/A
mcoln1b-F ACACGTTCGACATAGACCCTC mcoln1b-R TACCAACTTCTGAAAATTAAGGGTG	This publication	N/A
neu1-F ATGGGAAGTCATGGGAGAAG neu1-F TCCTCAGCAGAACCTCCTTT	This publication	N/A
psap-F CAGCAGCTCATGTCTATGGAACAG psap-R AGCAGGGATGGATTTGGCAGG	This publication	N/A
scpep1-F ATACAGCAGCAAAGGCAGTG scpep1-R TGTCATGGACCAAAGGTCAG	This publication	N/A
uvrag-F ACCGGAGGAAGAACAGTTTG uvrag-R CACACCTCAGAATCCCAATG	This publication	N/A
vps11-F GCACATCGACGACAATAACC vps11-R TCGTCTTCCTCAATCTGCTG	This publication	N/A
vps18-F ATGAACTGCCTGTCCAGTTG vps18-R ATATCGCCTCCTTGAAGTGG	This publication	N/A
vps8-F TGTCGGAGTCTTGTTTCTGC vps8-R TGGCTCATCCTCATCTTCAG	This publication	N/A
wipi1-F CAGATGGCTGGTCAGAGAAA wipi1-R TGAATAGCTGCCCATCAGAG	This publication	N/A
wipi2-F ACTTGGACGGGATACTTTGG wipi2-R AGCGCAGATGTTCTTGTGTC	This publication	N/A
Recombinant DNA		
Plasmid: *claudink:*Tfeb PN:polyA	This publication	N/A
Software and Algorithms		
GraphPad Prism	GraphPad Software	RRID:SCR_002798; URL: http://www.graphpad.com/
CLC Genomics Workbench 11.0	QiagenBioinformatics	RRID:SCR_011853; URL: http://www.clcbio.com/products/clc-genomics-workbench/

CONTACT FOR REAGENT AND RESOURCE SHARING

Further information and requests for resources and reagents should be directed to and will be fulfilled by the Lead Contact, William S. Talbot (william.talbot@stanford.edu).

EXPERIMENTAL MODEL AND SUBJECT DETAILS

Zebrafish

Zebrafish embryos, larvae and adults were produced, grown and maintained according to standard protocols approved by the Stanford University Institutional Animal Care and Use Committee. Ethical approval was obtained from the Stanford University Institutional Animal Care and Use Committee. To obtain embryos and larvae used in experiments, adults 3-18 months were crossed. Adult density was maintained at 5-10 fish/L, with a 14hr light/ 10nr dark cycle and fish were fed twice daily. Water temperature was maintained at 28°C. Embryos and larvae were treated with 0.003% 1-phenyl-2-thiourea (PTU) to inhibit pigmentation, and they were anesthetized with 0.016% (w/v) Tricaine prior to experimental procedures.

Published strains used in this study include: wildtype TL, *mtor*^{xu015} (Ding et al., 2011), *Tg(olig2:GFP)* (Shin et al., 2003), *Tg*(*cldnk:GFP*) (Münzel et al., 2012), *rraga*^{st77} and *lamtor4* $^{st99/st99}$ (Shen et al., 2016). Details of the construction of the new strains generated in this study are described below.

Mouse

Mice were housed and used according to standard UK Home Office regulations, under project license 60/ 4524 awarded to AW. 12-14 week old C57BL/6 male mice were used for all experiments. Experimental details are described below.

METHOD DETAILS

In Situ Hybridization

In situ hybridization on embryos and larvae was performed using standard methods (Thisse et al., 2004). Briefly, embryos were fixed overnight in 4% paraformaldehyde, dehydrated for at least 2 hr in 100% methanol, rehydrated in PBS, permeabilized with proteinase K, and incubated overnight with antisense riboprobes at 65°C. The probe was detected with an anti-digoxigenin antibody conjugated to alkaline phosphatase (11093274910, Sigma-Aldrich). Images were captured using the Zeiss AxioCam HRc camera with the AxioVision software. Probes for *mbp* and *olig2* were previously described (Lyons et al., 2009; Park et al., 2002). A 700 bp fragment of *plp1b* gene was amplified from 5 dpf whole larvae cDNA using the following primers: 5'- AACAGCCGTGGTTGTGTAAAGC-3' and 5'-TATGTTGGCCAGTGCATTTCCAC-3'. The resulting fragment was cloned into the pCRII vector using Dual promoter TA cloning Kit (K207020, Invitrogen) to generate a riboprobe for *plp1b*. The construct was linearized with SpeI and antisense probe was transcribed with T7 RNA polymerase (AM2085, Ambion). For each genetic cross, at least 3 independent clutches were analyzed. For each genotype a minimum of 10 total fish were analyzed.

Whole-Mount Immunofluorescence

For MBP immunofluorescence 8 dpf zebrafish larvae were fixed in 4%PFA/PBS, overnight at 4°C. Larval brains were dissected and incubated with rabbit anti-MBP (Lyons et al., 2005). Anti- rabbit Alexa Fluor568 was used at 1/1000 (A-11011, ThermoFisher). Embryos were mounted in DAPI Fluoromount-G (SouthernBiotech). Transgenic zebrafish embryos were mounted in 1.5% low melting point agarose in distilled water. Images were captured using a Zeiss LSM 5 Pascal or Zeiss LSM 7 microscope. Objectives used were Plan-Neofluar 10× (numerical aperture 0.30) and 20× (numerical aperture 0.75). All fish were genotyped after imaging and analysis.

Crispr/Cas9 Targeting

sgRNAs were designed using CHOPCHOP (https://chopchop.rc.fas.harvard.edu/, (Labun et al., 2016; Montague et al., 2014), transcribed with T7 polymerase (E2040S, New England Biolabs) and purified using mirVana miRNA isolation kit (AM1560, Ambion). Cas9 protein (Macrolab, Berkeley, http://qb3.berkeley.edu/macrolab/cas9-nls-purified-protein/) was injected together with 300 ng sgRNA into 1-cell stage embryos, and the embryos were genotyped after analysis to detect lesions. sgRNAs used were: TFEB (5'-GGTGCACTGATGGCTGGCGT-3').

tfeb mutant alleles were generated by raising embryos injected with sgRNA 5'-GGTGCACTGATGGCTGGCGT-3'. Two mutants were isolated and tested. *tfeb*^{st120} contains a 5 bp deletion which results in a change in reading frame after amino acid 45 and a premature stop codon after amino acid 61, compared to 491 amino acids for the WT protein. *tfeb*^{st121} contains a 8 bp deletion which results in a change in reading frame after amino acid 46 and a premature stop codon after amino acid 60. *tfeb* mutants were genotyped using the primers 5′- GCTCATGCGGGACCAAATGC -3′ and 5′- GGTCACACTAACAAATGTGG -3′. PCR products were digested with Cac8I (R0579, New England Biolabs). Mutant (233+83 bp) and WT (213bp + 83 +25 bp) bands were distinguished by running the digested PCR product on a 3% agarose gel. tfeb$^{st120/st120}$, tfeb$^{st121/st121}$ and tfeb$^{st120/st121}$ transheterozygotes all displayed equal phenotypes. All experiments were performed in transheterozygous fish.

FAC Sorting and RNA Sequencing

WT and *rraga*$^{-/-}$ mutant *Tg(cldnk:GFP)* larvae at 5 dpf were distinguished by neutral red staining and pooled for RNA isolation (Shen et al., 2016), in two independent experiments. Dissociation of embryos was carried out as previously described (Manoli and Driever, 2012) and GFP-positive cells were isolated at the Stanford Shared FACS Facility. RNA was isolated using the Qiagen RNeasy micro kit (74004, Qiagen) and provided to the Stanford Functional Genomics Facility. Libraries were prepared and sequenced using the Illumina NextSeq Mid platform.

qRT-PCR

Total RNA was extracted from larvae at 5 dpf with the RNAeasy kit (QIAGEN). cDNA was synthesized using iScript supermix (Biorad). qPCR was performed with SsoAdvancedTM Universal SYBR Green Supermix (Bio-Rad) on the Bio-Rad CFX384 Real-Time PCR Detection System. All experiments were done in biological and technical triplicates. Transcript levels were normalized to *ef1-alpha* (primers were previously reported (Shen et al., 2016; Shiau et al., 2013). Relative mRNA levels were calculated using ΔΔCT.

RNA-Seq Analysis

Over 7.5M paired end reads were obtained for each sample. These reads were mapped to the zebrafish reference genome (NCBI) using CLC Genomics Workbench 11.0 (http://www.clcbio.com/products/clc-genomics-workbench/) and over 90% of the sequenced fragments mapped to annotated genes. Differential expression analysis was performed by comparing the mapped WT and *rraga*$^{-/-}$ mutant reads, while controlling for the two independent experiments. Annotation was performed using the *Danio rerio* annotation file downloaded from Gene Ontology Consortium (http://www.geneontology.org/page/download-annotations). Raw and analyzed data were deposited with GEO: GSE119332.

Gene Ontology Enrichment

The list of 343 genes upregulated (p<0.01, >2,5X) in myelinating glia of *rraga*$^{-/-}$ was queried in PANTHER11 using gene ontology term cellular component (Mi et al., 2013, 2017).

Identification of Tfeb Targets in Genes Upregulated in *rraga*$^{-/-}$ Mutants

Significantly upregulated (p<0.01, >2.5X) and downregulated genes (p<0.01, <2.5X) in *rraga*$^{-/-}$ mutants were mapped to human orthologues using the Ensemble Biomart feature and compared to the list of TFEB targets (471 genes, (Palmieri et al., 2011)). 15 zebrafish genes orthologous to human Tfeb target genes were identified in the upregulated dataset, and 4 were identified in the downregulated dataset. Manual curation identified two additional upregulated genes with human TFEB target orthologues. Processing and analysis of gene lists was performed using Python.

Expression Constructs and Transient Injections

The coding sequence of *rraga* was cloned from 5 dpf embryonic cDNA pool and directionally inserted into pCR8/GW/TOPO vector (Invitrogen). Synthetic DNA encoding sequence of Tfeb (ENSDART00000182200.1) and Tfeb phosphorylation-null mutant was obtained from Integrated DNA Technologies (IDT) and subcloned into pCR8/GW by Gibson assembly (New England Biolabs). For transient transgenesis, *rraga*, *tfeb* and *tfeb* phospho-null sequences were subcloned into pDestTol2CG2 by multisite gateway. The tissue-specific regulatory sequences used have been reported elsewhere (Shen et al., 2016; Shiau et al., 2013). Tissue-specific transgenes were transiently expressed by co-injecting 12-25 pg of Tol2 plasmids described above and 100-200 pg of Tol2 transposase mRNA in 1 cell embryos.

Transmission Electron Microscopy

TEM was performed as described previously (Lyons et al., 2008). Briefly, decapitated embryos were fixed in 2% glutaraldehyde and 4% paraformaldehyde in 0.1 M sodium cacodylate buffer (pH 7.4). The posterior portion of the larvae was used to isolate DNA for genotyping. For secondary fixation, samples were fixed in 2% osmium tetraoxide, 0.1 M imidazole in 0.1 M sodium cacodylate (pH7.4), stained with saturated uranyl acetate, and dehydrated in ethanol and acetone. Fixation and dehydration were accelerated using the PELCO 3470 Multirange Laboratory Microwave System (Pelco) at 15°C. Samples were then incubated in 50% Epon/50% acetone overnight, followed by 100% Epon for 4 hr at room temperature. Samples were then embedded in 100% Epon and baked for 48 hr at 60°C. Blocks were sectioned using a Leica Ultramicrotome. Thick sections (500–1,000 μm) for toluidine blue staining were collected on glass slides, stained at 60°C for 5 s, and imaged with the Leica DM 2000 microscope using the Leica DFC290 HD camera and Leica Application Suite software. After the desired region of the spinal cord was reached, we collected ultrathin sections for TEM analysis on copper grids, and we stained them with uranyl acetate and Sato's lead stain (1% lead citrate, 1% lead acetate, and 1% lead nitrate). Sections were imaged on a JEOL JEM-1400 transmission electron microscope.

Drug Treatment

For Torin1 treatment, WT fish were incubated in 1 μM Torin1 (4247, Tocris Bioscience) in embryo water with PTU from 24 hpf to 5 dpf; fresh embryo medium, PTU and Torin1 were replaced daily.

LPC-Induced Demyelinating Lesions in Rodents

Focal demyelination was induced via stereotactic injection of L-α-Lysophosphatidylcholine (LPC, L4129, Sigma-Aldrich) into the *corpus callosum* of 12-14 week old C57BL/6 male mice (n=2-3 per time point). Anesthetized animals received 2μL of 1% LPC through a burr hole in the skull and at stereotactic coordinates 1.2 mm posterior, 0.5 mm lateral, 1.4 mm deep to the bregma over 4 minutes using a 30 gauge needle attached to a Hamilton syringe and driven by a Nano pump (KD Scientific Inc., Holliston, MA). The needle was additionally left on site for additional 4 minutes to avoid backflow. Similar stereotactic injection of PBS was followed to create a surgical control (PBS control). LPC causes reversible focal demyelination without axonal loss. The time course of de- and remyelination is well established and reproducible with demyelinated lesions appearing as early as 3 days post injection (3 dpi). Two time points with early (14 dpi) and late (28 dpi) remyelination were analyzed. Mice were subsequently perfused with 4% PFA, the brain tissue was harvested, cryoprotected in 30% sucrose and frozen embedded in OCT compound.

Immunohistochemistry of Mouse Tissue and Quantification

10 μm thick cryosections were briefly washed in PBS and microwaved for 10 minutes in Vector Unmasking Solution for antigen retrieval (H-3300, Vector) before blocking with 10% normal horse serum, 0.3% Triton-X in 1xPBS for 1 hr at RT. Sections were then incubated with primary antibodies in the same solution overnight at 4°C in a humidified chamber. Following washes in PBS, the cryosections were incubated with Alexa Fluor secondary antibodies (Thermo Fischer Scientific, 1:1000) for 1 ½ hrs at room temperature and counterstained with Hoechst for the visualization of the nuclei. Primary antibodies used: rabbit polyclonal anti-TFEB (Bethyl laboratories inc, A303-673A, 1:1000), mouse IgG anti-APC (CC1, OP80, Merck-Millipore, 1:500) and rat IgG2a anti-Myelin Basic Protein (clone 12, AbD Serotec, 1:300). All slides were mounted using mowiol mounting medium (475904, MERCK- Millipore) and imaged using Leica TCS SP8 confocal microscopy. From each section 3-5 random fields (145.31μm x 145.31μm each) were obtained. 2 sections were analyzed per animal. Total number of CC1/TFEB double positive oligodendrocytes was counted in lesion and perilesion areas (CC1+TFEB+/mm^2). For the same area, the number of CC1/TFEB double positive cells with high cytoplasmic

TFEB levels was also counted (CC1+ TFEB+ $^{\text{cytoplasmic high}}$/mm^2). Values for each sample were averaged, and data are depicted as mean percentage of CC1+ TFEB+ $^{\text{cytoplasmic high}}$/CC1+TFEB+ cells.

QUANTIFICATION AND STATISTICAL ANALYSIS

Sample sizes were chosen based on previous publications and are indicated in each figure and/or figure legend. No animal or sample was excluded from the analysis unless the animal died during the procedure. Except for electron microscopy samples, zebrafish larvae were only genotyped after image acquisition and analysis. EM samples were blinded before counts of myelinated axons numbers were performed. The experiments were not randomized. Sample sizes, statistical test and P values are indicated in the figures or figure legends. Statistical significance was assigned at $P < 0.05$. Statistical tests were performed using GraphPad Prism 6 or Prism 7 software.